High Resolution Impervious Surface Estimation: An Integration of Ikonos and Landsat-7 ETM+ Imagery

Rama Prasada Mohapatra and Changshan Wu

Abstract

Recent studies have attempted to extract impervious surfaces from high-resolution satellite imagery such as Ikonos and QuickBird. These images, however, often lack necessary spectral information due to technological limitations. This study integrates spectral information (temperature and moisture) derived from Landsat-7 ETM+ imagery with Ikonos imagery to derive high-resolution impervious surface information. Furthermore, three popular methods, including linear regression modeling, artificial neural network, and regression tree have been developed and compared using a paired t-test statistic. Analysis of results reveal that Tasseled Cap components particularly greenness and wetness of Ikonos imagery are most important in estimating sub-pixel imperviousness. Also, to some extent the brightness temperature derived from Landsat-7 ETM+ image helps in better estimation of impervious surfaces. Moreover, a comparative analysis indicates that the non-linear approaches yielded statistically better results. Particularly, the regression tree model generated best results with highest Pearson's r (0.939) and lowest mean absolute error (8.307).

Introduction

Currently, one of the notable changes on Earth's surface is urbanization. This gradually transforms natural landscapes to anthropogenic urban land uses, the majority of which are impervious surfaces. Defined as materials that do not absorb water, most of the anthropogenic impervious surfaces are urban infrastructures that include roads, sidewalks, parking lots, and various rooftops (Arnold and Gibbons, 1996). With rapid urbanization, these anthropogenic impervious surfaces are increasing on a regular basis (Hasse and Lathrop, 2003; Xian *et al.*, 2008; Powell *et al.*, 2008; Esch *et al.*, 2009). For instance, the impervious surface area in Rhode Island increased 43 percent from 1972 to 1999, and as of 2004, 10 percent of the state was covered by impervious surfaces (Zhou and Wang, 2007). When the conterminous United States is considered, it is estimated that the aggregate impervious surface area is slightly over one percent of the total land area, roughly equivalent to the size of the State of Ohio (Elvidge *et al.*, 2004). Although impervious surfaces only cover a small geographical area, they have significant influence on urban and natural environments. Impervious surfaces modify the energy balance of a geographic area and lead to higher temperatures in urban areas than in rural areas (Xian and Crane, 2006; Xian, 2008; Weng and Lu, 2008). Moreover, impervious surfaces prohibit the penetration of water into soil, and contribute to environmental hazards such as flooding (U.S. EPA, 2008). In addition, the increase in impervious surface area boosts the transportation and accumulation of non-point pollutants from surface runoff (Xian *et al.*, 2007). Because of their importance to urban and natural environments, quantification of impervious surfaces has become an important research agenda (Civco *et al.*, 2002; Wu, 2004; Dougherty *et al.*, 2004; Xian and Crane, 2005; Yang, 2006; Lu and Weng, 2006; Yuan and Bauer, 2007; Xian *et al.*, 2008, Chabaeva *et al.*, 2009; Weng and Lu, 2009).

Although surveys and digitization over aerial photographs are the most accurate methods of mapping impervious surfaces, it is time consuming and labor intensive, in particular for a large study area (Zhou and Wang, 2008). In this context, as satellite remote sensing data offers timely synoptic view over large geographical areas, recent studies have focused on automated extraction of impervious surfaces by classification of remote sensing imagery (Yuan *et al.*, 2008). In a majority of these studies, moderate resolution remote sensing data, such as Landsat Thematic Mapper and SPOT MSI imagery, have been employed. However, moderate resolution remote sensing imagery is not the best solution for fine scale urban applications due to their coarse resolutions, and thereby not preferred by urban planners and policy makers (Mesev, 1997; Carlson, 2003). With the advancement in high-resolution satellite remote sensing technologies, in particular since the availability of Ikonos and QuickBird imagery, mapping impervious surfaces at finer scales with frequent intervals has become possible. Therefore, recently, a few studies have attempted to extract impervious surfaces from high-resolution remote sensing imagery with different degrees of success (Cablk and Minor, 2003; Goetz *et al.*, 2003; Small, 2003; Yuan and Bauer, 2006; Mohapatra and Wu, 2007; Hester *et al.*, 2008; Zhou and Wang, 2008; Zhang *et al.*, 2009; Lu and Weng, 2009; Wu, 2009). Goetz *et al.* (2003) extracted impervious surfaces from Ikonos imagery with the help of Normalized Difference Vegetation Index (NDVI) and band ratios (NIR/Red, NIR/Blue, and NIR/Green). Cablk and

Rama Prasada Mohapatra and Changshan Wu are with the Department of Geography, University of Wisconsin- Milwaukee, Milwaukee, WI 53201 (rama@uwm.edu).

Photogrammetric Engineering & Remote Sensing
Vol. 76, No. 12, December 2010, pp. 000–000.

0099-1112/10/7612–0000/$3.00/0

Minor (2003) identified impervious surfaces from the panchromatic and multispectral images of Ikonos using morphological operators. The study also derived four principal components of Ikonos image to examine how impervious surfaces are represented in each principal component. Hester *et al.* (2008) used ancillary GIS data to eliminate confusion between impervious surface and water. Zheng *et al.* (2005) distinguished roads from rivers with the fractal dimensions derived from an Ikonos image. Lu and Weng (2009) extracted water, shadows, and impervious surface information and argued that the limited spectral information of high-resolution data limits accurate extraction of impervious surfaces. Moreover, several studies reveal that the spectral variability within land cover types increases with fine resolution particularly in highly heterogeneous urban environments (Small, 2003; Herold *et al.*, 2004; Lu and Weng, 2009; Wu, 2009). In addition, when applied to urban areas, land-use classification accuracy decreases due to the spectral overlap between soil and impervious surface (Hester *et al.*, 2008).

Unlike medium resolution remote sensing data, high-resolution remote sensing imagery provides much more spatial details but lacks necessary spectral information (Thomas *et al.*, 2003; Goetz *et al.*, 2003; Herold *et al.*, 2004). Currently available high-resolution remote sensing imagery, such as Ikonos and QuickBird have only visible (VIS) and near-infrared (NIR) bands, and lacks shortwave infrared (SWIR) and thermal infrared (TIR) bands due to technological limitations of remote sensors. For urban applications, SWIR and TIR spectra may be important to separate impervious surfaces from other land-cover types (Herold *et al.*, 2004; Warner and Nerry, 2009). SWIR bands are important to extract water (surface moisture) information, and TIR bands are essential for obtaining surface temperature information. Information related to water content and surface temperature may be essential to separate impervious surfaces from other land-cover types. When compared to bare soil, as an example, impervious surfaces may contain less water and have a higher temperature during the daytime. Therefore, for better estimation of high-resolution impervious surface information, it is necessary to integrate spectral information obtained from medium-resolution remote sensing imagery. Little research, however, has been conducted to incorporate the spectral information (e.g., SWIR and TIR) from medium-resolution data to facilitate impervious surface extraction from high-resolution remote sensing imagery.

This study extracted two spectral parameters, brightness temperature and Normalized Difference Water Index (NDWI), from Landsat-7 ETM+ imagery and integrated them with Ikonos imagery to derive high-resolution impervious surface information. Three popular sub-pixel classification approaches, regression modeling, artificial neural network (ANN), and regression tree, were developed for impervious surface extraction. Results of these approaches were evaluated and compared using a paired *t*-test statistic. The objectives of the study are: (a) to utilize brightness temperature and NDWI obtained from Landsat-7 ETM+ along with spectral and spatial information of Ikonos imagery to extract sub-pixel imperviousness, and (b) to compare linear (regression model) and non-linear (artificial neural network and regression tree) approaches for high-resolution sub-pixel impervious surface estimation. The remainder of this paper is organized as follows. The next section describes the study area and data, followed by the information extracted from Ikonos and Landsat-7 ETM+ data. Then, the methodology of this research, including regression modeling, ANN, and regression tree analysis for impervious surface estimation, followed by reports of the modeling results, and finally, the conclusions.

Study Area

For this research, Grafton Village and Township (see Figure 1) in Ozaukee County, Wisconsin, was chosen as the study area. This area is covered by a variety of urban (e.g., residential, commercial, transportation, etc.) and rural (e.g., agriculture and forestry) land uses. The total estimated land area of Grafton excluding water bodies is roughly twenty four square miles (U.S. Census, 2000). According to the South Eastern Wisconsin Regional Planning Commission (SEWRPC), the study area experienced rapid growth in terms of population and housing unit numbers from 1970 to 2000. The population in the village almost increased 58 percent and the number of housing units doubled in the same time period; this trend is likely to continue (SEWRPC, 2004).

An Ikonos image acquired on 03 September 2002 was obtained from the American Geographical Society Library (AGSL) at the University of Wisconsin-Milwaukee. A Landsat-7 ETM+ image for the same time period of the year was also collected from **www.wisconsinview.org**. The Ikonos image (4-meter resolution) comprises of four bands (blue, green, red, and NIR). For the Landsat-7 ETM+ image, the spatial resolution for bands 1 through 5 and 7 is 28.5 meters, and band 6 has a resolution of 57 meters. The Ikonos and Landsat-7 ETM+ images were utilized to derive impervious surface information. In addition, a color aerial photograph, with a resolution of two feet, was also obtained from the AGSL. This photograph was employed to select training and testing samples, and to examine the accuracy of impervious surface estimation. All the images were re-projected to the UTM projection (WGS84, Zone 16). No geometric corrections were performed since no significant mis-registration was found. As the study area is small and major atmospheric effects were not evident, atmospheric corrections were not carried out.

Remote Sensing Information

Information Extraction from Ikonos Data

In this paper, both spectral and spatial information were derived from the Ikonos image to estimate impervious surface distribution. For spectral information, Tasseled Cap components have been typically employed for extracting impervious surfaces (Yuan and Bauer, 2006 and 2007). In particular, the greenness (the second component of Tasseled Cap transformation) has proven to have a significant and negative correlation with impervious surfaces. In addition to spectral information, spatial information such as texture has also been applied to separate impervious surfaces from other urban land covers. In fact, fractal dimension analysis has proven effective for analyzing urban land uses (Zheng *et al.*, 2005). Therefore, in this study, we derived both Tasseled Cap components and fractal dimension from the Ikonos image.

Spectral Information: Tasseled Cap Components

Proposed initially by Kauth and Thomas (1976), Tasseled Cap transformation is generally performed to transform '*n*' dimensional Landsat TM data into new '*n*' dimensional components for spectral information enhancement. The three major components produced from the Tasseled Cap transformation are brightness, greenness, and wetness. Brightness shows principal variation in soil reflectance, greenness is related to green vegetation, and wetness indicates information about canopy and soil moisture (Jensen, 2007). While the initial Tasseled Cap transformation was proposed for Landsat TM data, subsequently similar transformations were developed for different sensors. When applied to Ikonos imagery, Horne (2003) developed a Tasseled Cap transformation and examined its validity by testing over two hundred

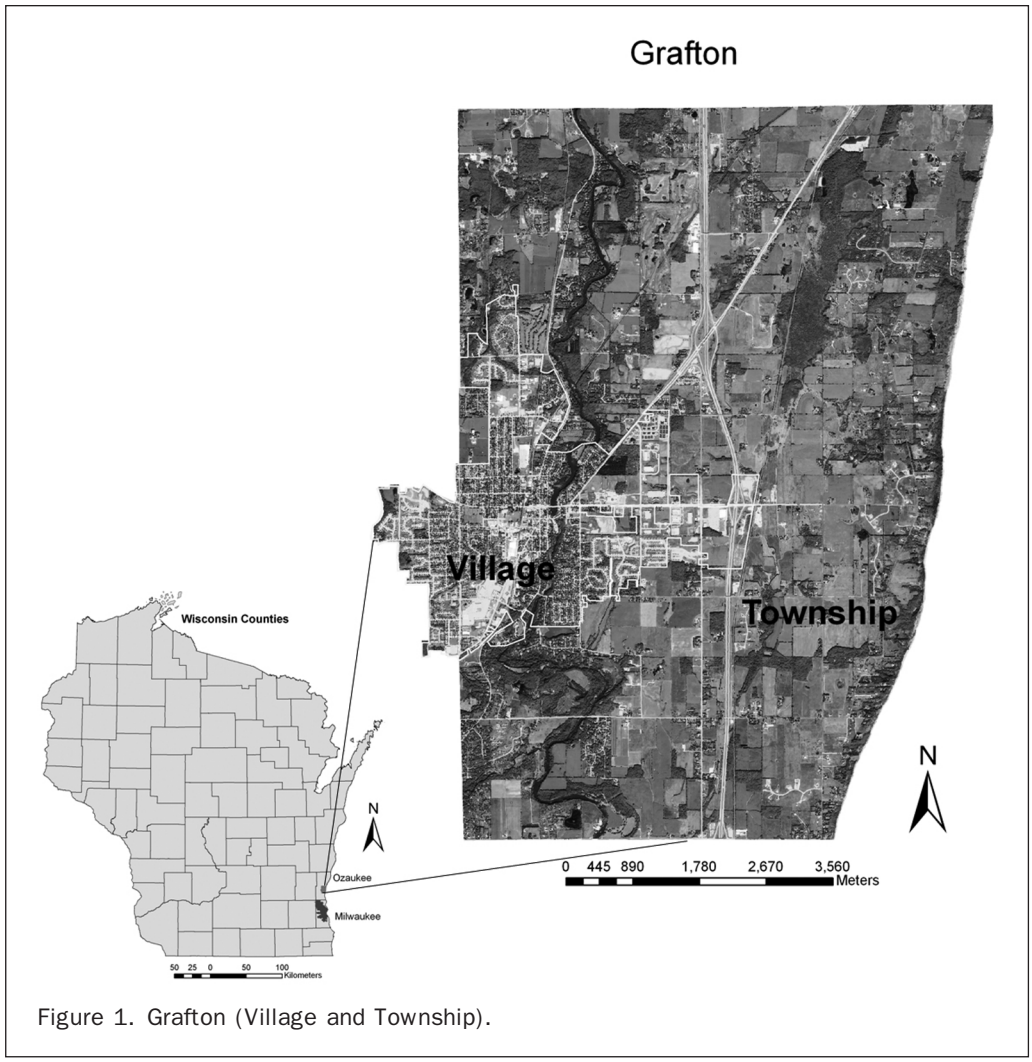

Figure 1. Grafton (Village and Township).

Ikonos images globally. Following the approach of Horne (2003), this paper generated four Tasseled Cap components, with the first three representing brightness, greenness, and wetness (see Figure 2). Although they bear the same name, the original Tasseled Cap transformation proposed for Landsat data includes shortwave infrared bands which are not available for Ikonos imagery. Therefore, it is expected that the Tasseled Cap components obtained from Ikonos data would be different. It has been established that Tasseled Cap component 2 (greenness) of Landsat image could explain almost all the variation in impervious surfaces (Bauer *et al.*, 2004). However, it is yet to be explored for the Ikonos data, particularly for estimating imperviousness. Therefore, in this study, all these four Tasseled Cap components were employed for impervious surface estimation.

Spatial Information: Fractal Dimension

In addition to spectral enhancement, texture analysis was also applied to the Ikonos image. Texture information measures the variability in digital number (DN) values within a group of pixels. Various methods, such as local variability, variograms, fractal dimension, etc. have been proposed for extracting texture information from satellite images. Among them fractal dimension seems to be very appealing as it could be applied at various scales (Emerson *et al.*, 1999). The concept of fractal dimension is based on a perimeter-area calculation method (Mandelbrot, 1982) in order to quantify the degree of complexity of the planar shapes. This not only explains the complexity of shapes but also exhibits the property of self-similarity statistically. Commonly, fractal dimension is measured by measuring the length of a section of a feature with varying precision. If the form is fractal then there exists a linear relationship between precision and length in a log/log plot. In this study, a different procedure based on the logic of Eastman (1985) which considers the slope of each segment of the log/log plot to provide evidence of an underlying angularity to estimate the fractal dimension was used (Eastman, 2003). In order to calculate the fractal dimension, principal component analysis was carried out over the Ikonos image and the first principal component was used. The TEXTURE tool in IDRISI Andes was used to obtain the fractal dimension image (see Equation 1 and Figure 3).

$$f = \frac{\log 2}{\log 2 + \log\left(\sin\left(\frac{180 - slope}{2}\right)\right)} \quad (1)$$

where, f is the fractal dimension for a pixel, and *slope* is calculated in degrees for the same pixel based on a 3×3 window.

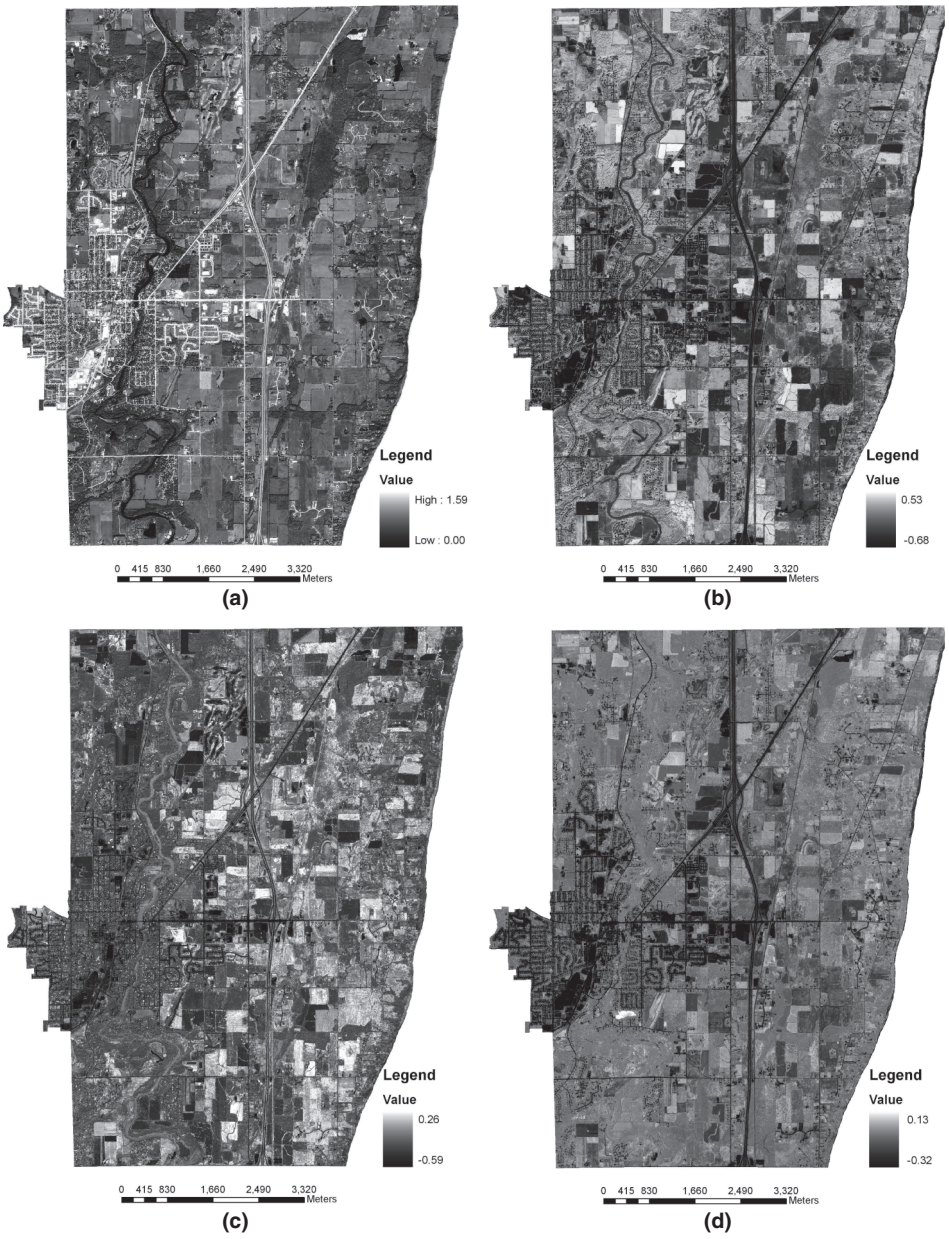

Figure 2. Tasseled Cap Components of Ikonos Image: (a) Tasseled Cap Component 1 (Brightness), (b) Tasseled Cap Component 2 (Greenness), (c) Tasseled Cap Component 3 (Wetness), and (d) Tasseled Cap Component 4 (Fourth).

Information Extraction from Landsat-7 ETM+ Data

Besides information from the Ikonos image, two parameters, brightness temperature and NDWI, were derived from the Landsat-7 ETM+ image. The purpose of generating these two parameters is to evaluate whether the spectral information from Landsat-7 ETM+ image can contribute to a better estimation of impervious surfaces from the high-resolution Ikonos image.

Temperature Estimation

Brightness temperature was derived from the Landsat-7 ETM+ TIR band. Two steps described in the Landsat-7 ETM+ user manual were followed to calculate the brightness temperature. The first step involves the conversion from digital numbers (DNS) to spectral radiances, and the second step is to calculate the brightness temperature from the spectral radiances assuming a uniform emissivity applied for different land covers (see Equation 2).

$$T = \frac{K_2}{\ln\left(\frac{K_1}{L_\lambda} + 1\right)} \quad (2)$$

where T is at satellite temperature in Kelvin, L_λ is the pixel value as radiance, and K_1 and K_2 are pre-lunch calibration constants for Landsat-7 ETM+

After calculating the brightness temperature for each pixel, a nearest neighbor interpolation technique was carried

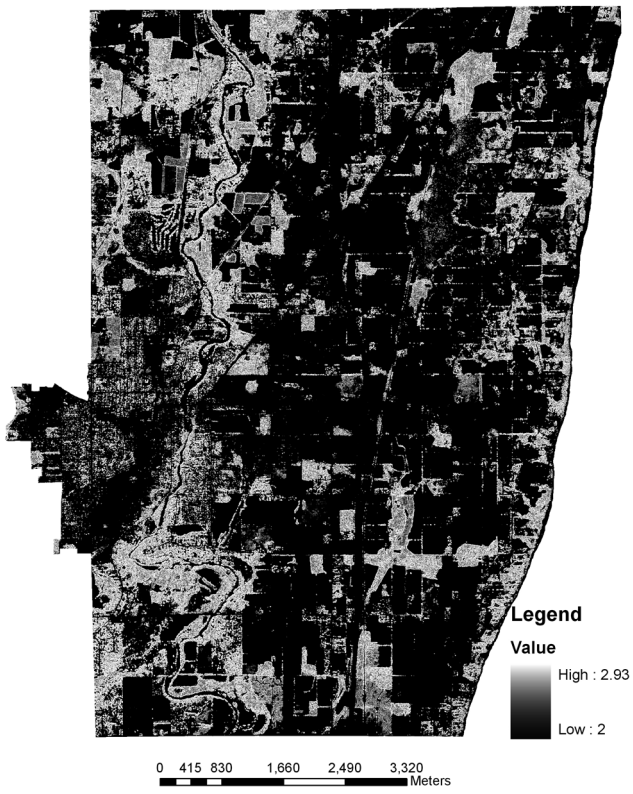

Figure 3. Fractal Dimension Image.

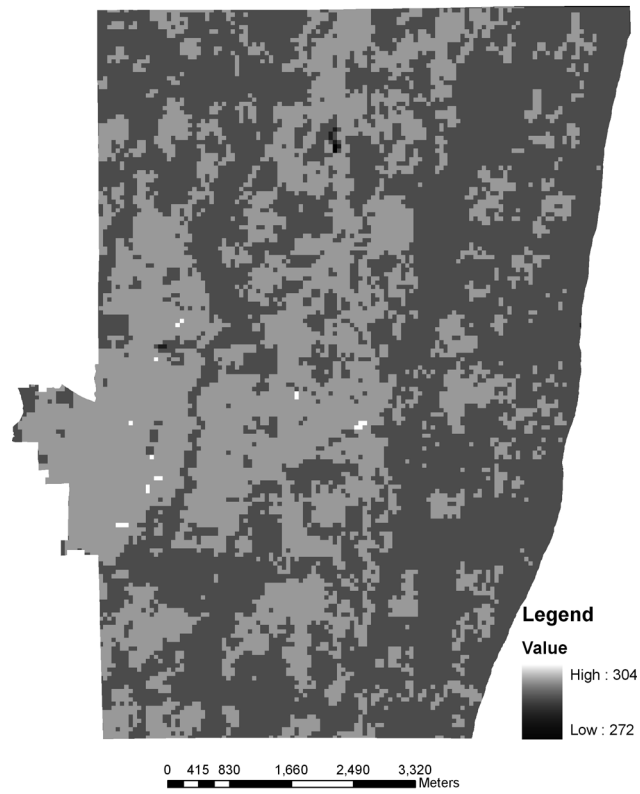

Figure 4. Brightness Temperature Image.

out to resample the pixel size to 4 m by 4 m to match the pixel size of the Ikonos image (see Figure 4).

Water Information: Normalized Difference Water Index (NDWI)

Many studies have attempted to estimate water content using satellite remote sensing reflectance data (Jackson *et al.*, 2004). Water strongly absorbs the radiances in SWIR bands, and reflects the majority of radiances in NIR bands. Therefore, the combination of SWIR and NIR spectra was typically utilized to represent water content. In particular, Gao (1996) developed the NDWI to relate Landsat TM reflectance spectra to water content (see Equation 3).

$$NDWI = \frac{R_{NIR} - R_{SWIR}}{R_{NIR} + R_{SWIR}} \quad (3)$$

where, *NDWI* is normalized difference water index, and R_{NIR} and R_{SWIR} correspond to the reflectance in band 4 and band 5 of Landsat-7 ETM+ image, respectively.

As NDWI is related to water content, it might be helpful in differentiating impervious surface from soil with some water content. Therefore, in this paper, the NDWI was calculated for each Landsat-7 ETM+ pixel, and resampled to the size of Ikonos pixels (see Figure 5).

Methodology

With the above parameters extracted from Ikonos and Landsat-7 ETM+ data, it is necessary to apply them to model impervious surfaces. In this paper, three models, regression modeling, ANN, and regression tree method were applied to estimate high-resolution impervious surfaces.

Regression Modeling

Initially, ordinary least squares (OLS) regression models were utilized to explore the relationship between percentage imperviousness and the parameters extracted from the satellite data, including the Tasseled Cap components and fractal dimension from the Ikonos image, and brightness temperature and NDWI obtained from the Landsat-7 ETM+ data. Then, stepwise regression analysis was performed in SPSS 17.0 statistical analysis software to explore the explanation power of individual independent variables. Subsequently, the independent variables which are not statistically significant were ignored and two regression models were constructed to estimate the sub-pixel imperviousness of the entire image. In the first model, parameters extracted from the Ikonos image were employed as independent variables, whereas in the second model, additional variables obtained from the Landsat ETM+ data were added. These two model results were later compared to specifically evaluate the contribution of Landsat ETM+ data in estimating imperviousness. The formulation (see Equation 4) of the model is as follows:

$$I = \sum_i \alpha_i \times TC_i + \beta \times Fractal + \gamma \times Temp + \delta \times NDWI + \varepsilon \quad (4)$$

where, I is the percentage impervious surface for an individual pixel, *TCi* is the i^{th} Tasseled Cap component of the Ikonos image, *Fractal* is the fractal dimension extracted from the Ikonos image, *Temp* and *NDWI* are the brightness temperature and normalized difference vegetation index, respectively, obtained from the Landsat-7 ETM+ image (for the second model), and α, β, γ, δ, and ε are regression coefficients.

Figure 5. Normalized Difference Water Index Image.

Artificial Neural Network Classification

Unlike the linear regression model, ANN provides an alternative to traditional statistical classification approach as it is more flexible and could map nonlinearity among variables without assumptions about the data (Ji, 2000). Furthermore, ANN has proven to be superior while classifying per-pixel Landsat data over other classifiers such as maximum likelihood (Flanagan and Civco, 2001; Kavzoglu and Mather, 2003; Wang *et al.*, 2008), and also outperform the traditional linear unmixing models (Liu and Wu, 2005). Earlier studies have revealed that ANNS could analyze complexity including nonlinearity in urban areas and estimate fractional biophysical information such as impervious surfaces from moderate (Civco and Hurd, 1997) and high-resolution satellite imagery (Mohapatra and Wu, 2007). ANNS were also used to classify land-cover types from Landsat-7 ETM+ data using additional data such as texture and topographic information (Aitkenhead, 2008).

In this study, the proportions of vegetation, impervious surface, and soil (VIS) within each individual pixel of the Ikonos image were estimated through ANN classification following the method proposed by Mohapatra and Wu (2007). The four Tasseled Cap components, fractal dimension, brightness temperature, and NDWI were employed as inputs in the neural network structure (see Figure 6) where the three output nodes represented vegetation, impervious surface, and soil. Similar to the regression analysis, two neural network models were created, with the first model only utilizing the variables extracted from the Ikonos data and the second model employing all variables derived from the Ikonos and Landsat ETM+ image. The Multi-Layer Perceptron (MLP) classifier module of IDRISI Andes, which employs the widely used back propagation learning algorithm (Eastman, 2003), was utilized to obtain the sub-pixel VIS information. When an input pixel is presented to MLP classifier, each output node is assigned a value that is

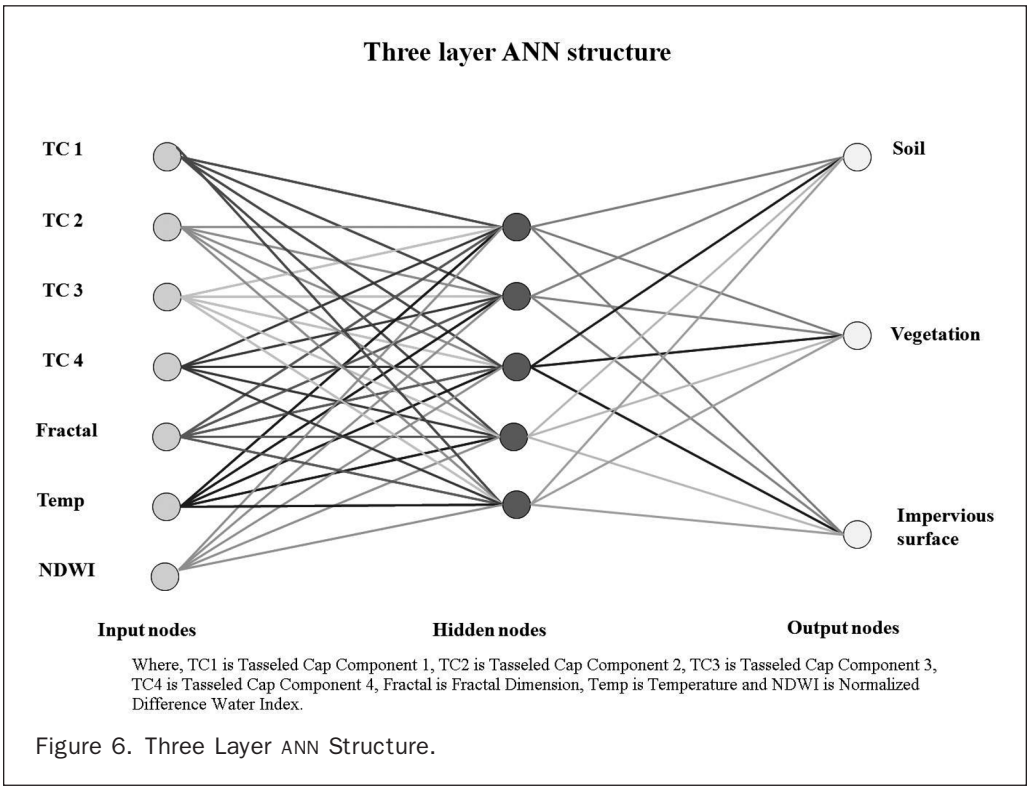

Figure 6. Three Layer ANN Structure.

compared to the expected value. When the output result achieves a predefined accuracy level, the input pixel is assigned an activation value ranging between 0 to 1 where larger values represent a higher degree of membership (Kavzoglu and Mather, 2003; Eastman, 2003; Mertens *et al.*, 2004) belonging to that corresponding node (vegetation or impervious surface or soil).

To achieve higher accuracies through MLP classifier it is necessary to design the optimum network structure (see Figure 6) and set proper learning parameters. While deciding the optimum network structure, the number of hidden layer nodes is the most important and were estimated using the following equation (see Equation 5):

$$N_h = INT\sqrt{N_i \times N_o} \tag{5}$$

where, N_h is the number of hidden layer nodes, N_i is the number of input layer nodes, and N_o is the number of output layer nodes.

Besides neural network structure, several other parameters influence the performance of the ANN classifier such as sigmoid function constant, learning rate, and momentum factor which were decided following the suggestions of Kavzoglu and Mather (2003).

Classification and Regression Tree Analysis

Like ANN classifiers, the classification and regression tree (CART) technique has been widely used in satellite image processing and proven effective in generating impervious surface information in urban areas. CART is a tree building technique to predict a dependent variable (percentage imperviousness) based on the independent variables. CART can select few important variables and their interactions from a large number of variables submitted for analysis. CART technology is inherently non-parametric and is not restricted to the assumptions of normal distribution of independent or dependent variables, multi-collinearity among independent variables, issues of heteroskedacity, etc. The classification and regression tree technique has the ability to handle both categorical (classification tree) and continuous (regression tree) dependent variables. Depending on how the independent and dependent variables interact with each other, the CART technology grows a binary tree by repeatedly splitting the data. As the technology is based on a binary partitioning, the pixels under consideration can only be split into two more or less homogenous groups again and again until all the pixels are classified into one category or the other uncovering the predictive structure of the problem under consideration (Breiman *et al.*, 1984). Regression tree models have been successfully applied to both medium and high-resolution satellite imagery to extract impervious surface fraction (Yang *et al.*, 2003, Lu and Weng, 2009).

In this study, a regression tree program, Cubist, developed by Quinlan (1993) was utilized to model the percentage impervious surface (dependent variable) against independent variables such as four Tasseled Cap components of the Ikonos image, fractal dimension derived from the Ikonos image, brightness temperature, and NDWI information derived from the Landsat-7 ETM+ data. Similar to the previous two modeling approaches, one model with Ikonos related variables only, and the other with parameters from both Ikonos and Landsat ETM+ imagery were constructed.

Accuracy Assessment and Model Comparison

For regression and regression tree methods, 300 samples were generated using a stratified random sampling methodology ensuring enough samples in the urban areas. A 5 by 5 sampling size was utilized to diminish the effects caused by image mis-registration. Within these 300 samples, 150 were utilized for model development and the other 150 were applied for accuracy assessment. For training and testing MLP classifier, for each of the land-cover classes (vegetation, impervious surface, and soil) 30 sampling sites were selected so that they could represent the spectral and spatial variations of the entire image. After obtaining the impervious surface fraction from MLP classifier, in order to compare the ANN result with the other two model results, the same 150 samples which were used for accuracy assessment of regression, and regression tree methods were also used for accuracy assessment of the ANN method. While assessing accuracy, for each sampling point (5 pixels $\times$ 5 pixels of Ikonos image), the actual imperviousness was calculated with the help of the color aerial photograph and was compared with the estimated imperviousness. In particular, for a sampling point, the total area of impervious surface within the 5 pixels by 5 pixels (20 m by 20 m) of Ikonos image was manually digitized; the percentage of impervious surface area to the total sampling area (400 square meters) was calculated. After obtaining the estimation for the actual imperviousness and estimated imperviousness, two quantitative estimators were utilized to compare the results obtained through regression, ANN and regression tree methods. The first estimator is the Pearson's correlation coefficient (Pearson's *r*) and second one is the mean absolute error (*MAE*). Pearson's *r* is a measure of reliability and describes the strength of relationship between the actual and estimated imperviousness. The *MAE* (Equation 6) is about the relative prediction error which is estimated as follows:

$$MAE = \frac{1}{N}\sum|I_i - \hat{I}_i| \tag{6}$$

where, I_i is the actual imperviousness for sampling unit i obtained from color aerial photograph, $\hat{I}_i$ is the estimated imperviousness for the same sampling unit i, and N is the total number of samples.

In addition to the Pearson's *r* and *MAE* measurements, a paired *t*-test was also performed on the residuals of all the methods. The paired sample *t*-test was conducted to determine (a) whether additional information from Landsat ETM+ data is helpful in improving the imperviousness estimation, and (b) if there is a significant difference between the mean absolute errors of imperviousness measurement and evaluate whether a particular model is significantly better than others. To achieve the first goal, the two modeling results, one with only Ikonos data and the other with both Ikonos and Landsat data, of the three methods were compared using a paired sample *t*-test. Then, following the similar *t*-test approach, the results of all the three methods (regression, ANN, and regression tree) were compared to determine whether the imperviousness derived from one method is significantly different from those generated by other methods. Particularly, the mean absolute error and the *t* value along with significance level (*p* value) were obtained for comparing the pairs.

Results and Discussion

Impervious Surface Extraction

Regression Modeling

Results of regression modeling (see Table 1) suggest that three independent variables, Tasseled Cap component 2 and Tasseled Cap component 3 from Ikonos data, and brightness temperature from the Landsat-7 ETM+ image, are closely

TABLE 1. RESULTS OF FINAL REGRESSION MODELS

Model 1: Only Ikonos Data				
	B	Std. Error	*t*	*Sig.*
(Constant)	18.34	1.73	10.604	0.000
TC2	-116.6	6.557	-17.784	0.000
TC3	-514.58	39.274	-13.102	0.000
Model 2: Ikonos and Landsat ETM+ Data				
	B	Std. Error	*t*	*Sig.*
(Constant)	-223.21	96.62	-2.31	0.022
TC2	-109.7	7.01	-15.65	0.000
TC3	-508.66	38.66	-13.16	0.000
TEMP	0.82	0.33	2.5	0.014

Where, TC2 and TC3 are Tasseled Cap components 2 and 3, respectively, and TEMP is Brightness. Temperature obtained from Landsat ETM+

related to the percentage imperviousness. Moreover, it indicates that approximately 80 percent of the variation in the percentage imperviousness (see Figure 7b) can be explained by these three variables (R^2 = 0.802). If the contribution of brightness temperature is ignored (see Figure 7a) then approximately 79 percent of the variation in the percentage imperviousness can be explained. In the regression models, other explanatory variables, including Tasseled Cap component 1, Tasseled Cap component 4, and fractal dimension from Ikonos and NDWI from Landsat-7 ETM+ image, were not statistically significant in improving the model estimates.

Additionally, a forward stepwise regression model was constructed to examine if a particular variable significantly improves the model predictability where the R^2 change statistic and *F* statistic were used as the criteria. The R^2 change statistic and associated significance of *F* change were helpful in deciding if inclusion of independent variables such as temperature obtained from Landsat ETM+ is helpful in significantly improving the model estimates. Results (see Table 2) reveal that Tasseled Cap component 2 is the most important explanatory variable which explains approximately 55 percent of the variation in percentage imperviousness by itself (R^2 = 0.552). This suggests that Tasseled Cap component 2 of Ikonos image or greenness is strongly related with the amount of green vegetation and inversely related to the amount of impervious surface. This result is consistent with the previous studies applied to medium resolution satellite data (Bauer *et al.*, 2004). However, unlike Landsat data besides Tasseled Cap component 2, Tasseled Cap component 3 of Ikonos image also plays a very significant role in explaining the variation in percentage impervious surface. By including Tasseled Cap component 3 in the model, the R^2 increases by 0.241 to 0.793 which is highly significant (significant (0.000) *F*-value change). Tasseled Cap component 3, which can be explained as wetness or soil moisture, is negatively correlated with impervious surfaces, and is important in identifying impervious surfaces. In addition to these parameters from Ikonos imagery, the brightness temperature from Landsat-7 ETM+ data, also significantly improves the model performance (significant (0.014) *F*-value change) although the R^2 change is only 0.008. As temperature increases with the intensity of imperviousness, it is positively correlated with impervious surfaces.

Artificial Neural Network

After several attempts of running the MLP classifier it was found that a learning rate of 0.0083 and momentum factor of 0.56 yields the best result. The 95 percent accuracy cut off was used to terminate the MLP classifier. It was found that inclusion of fractal dimension and NDWI decreased the overall accuracy of MLP classifier and could not attain the 95percent cut off accuracy. So it was decided not to consider them as input layers in the final models. For both the models, one with only Ikonos data (see Figure 7c) and the other with both Ikonos and Landsat ETM+ data (see Figure 7d), the MLP classifier produced as many images (activation level maps) as the total number of nodes (three) in the output layer by assigning the pixels the highest activation value of each node. For this study, only the activation level map representing the impervious surface fraction of the two models (see Figure 7c and 7d) were considered for comparison and accuracy assessment. The output values of the activation level map obtained from the MLP classifier ranges between 0 to 1 representing the degree of membership of imperviousness or the likelihood of a pixel belonging to the land-cover class impervious surface. So it could be inferred that this likelihood should closely relate to the percentage imperviousness within the pixel. Hence, there should be a close relationship between the actual sub-pixel imperviousness and the estimated sub-pixel imperviousness through ANN classification. For comparing the ANN classification result with the actual imperviousness at first, the activation values were converted to percentage and then compared with the actual imperviousness.

Classification and Regression Tree

With the Cubist program, the regression tree model was developed. The conditions (rules) and coefficients of independent variables and their relative importance are showed in Table 3, and the percentage imperviousness image is displayed in Figure 7e. Analysis of results suggest that the Tasseled Cap components particularly Tasseled Cap component 2 (greenness) and Tasseled Cap component 3 (wetness) are better predictors while estimating sub-pixel imperviousness from Ikonos image. It was found out that with this approach, fractal dimension, brightness temperature, and NDWI information are not helpful in estimating sub-pixel imperviousness. So the resultant model uses only Ikonos data.

Accuracy Assessment and Model Comparison

Comparison between Models Without and With Landsat Information

In order to evaluate the contribution of Landsat-derived information in discriminating impervious surface, the modeling accuracy of each method without and with Landsat information was calculated and compared. In particular, the Pearson's *r* and *MAE* measurements for each method were calculated using the testing samples (see Table 4 and Figure 8). In addition, the paired *t*-test was carried out to examine whether the improvements due to the addition of Landsat derived information are statistically significant.

By comparing the correlation coefficient (*r*) and *MAE* for each individual method, it was found out that for regression analysis and ANN, the addition of brightness temperature improves the accuracy of impervious surface estimation. The *t*-test results suggest that the two regression models, one employing Ikonos data only (r = 0.915, *MAE* =10.913) and the other utilizing both Ikonos and Landsat ETM+ data (r = 0.918, *MAE* = 10.622) are not significantly different (t = *1.408,* p = 0.161) from each other. When the two ANN models were compared, the one with Ikonos data only (r = 0.924, *MAE* = 12.208) was significantly worse (t = 4.461, p = 0.000) than the counterpart with both Ikonos and Landsat ETM+ information

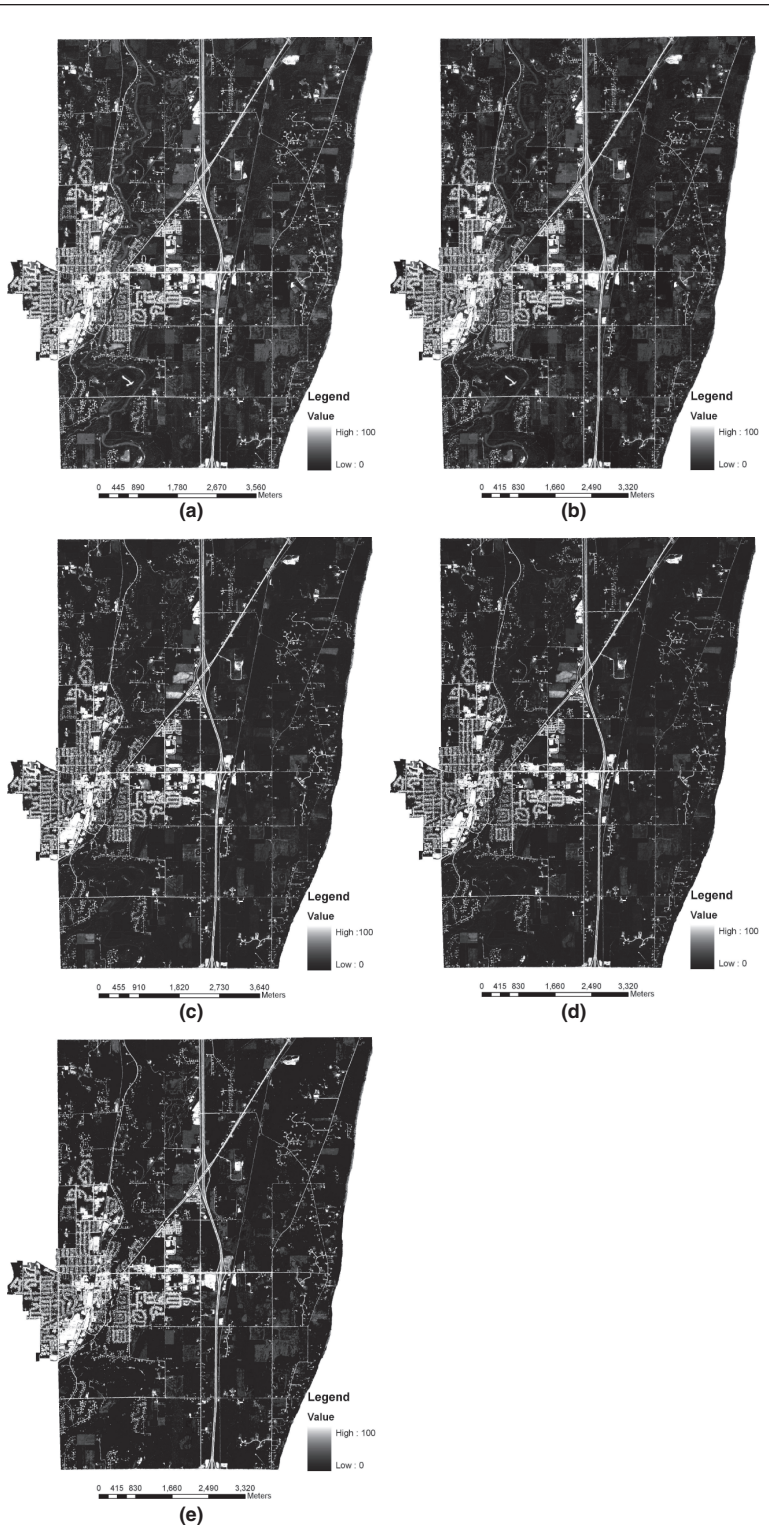

Figure 7. (a) Estimated Impervious Surface Fraction through Regression (Only Ikonos data), (b) Estimated Impervious Surface Fraction through Regression (Ikonos and Temperature data), (c) Estimated Impervious Surface Fraction through ANN (Only Ikonos data), (d) Estimated Impervious Surface Fraction through ANN (Ikonos and Temperature data), and (e) Estimated Impervious Surface Fraction through Regression Tree (Only Ikonos data). Estimated Impervious Surface Fraction through Regression (7a and 7b), Neural Network (7c and 7d), and Regression Tree (7e)

TABLE 2. RESULTS OF FORWARD STEPWISE REGRESSION MODEL

		Change Statistics		
R	R Square	R Square Change	F Change	Sig. F Change
.743(a)	0.552	0.552	182.483	0.000
.891(b)	0.793	0.241	171.673	0.000
.895(c)	0.802	0.008	6.251	0.014

Where:
a. Predictors: (Constant), TC2
b. Predictors: (Constant), TC2, TC3
c. Predictors: (Constant), TC2, TC3, TEMP
TC2, TC3 and TEMP is Tasseled Cap component 2, 3 and Temperature, respectively.

TABLE 3. RULE DEFINITION USING THE REGRESSION TREE MODEL

Rule	Condition	Impervious Surface Fraction
1	TC4 >-0.033	1.42178
2	TC4 <=-0.033	36.637 - 112 TC2 - 667 TC3 - 31 TC1

Where, TC1, TC2, TC3, and TC4 are Tasseled Cap components 1, 2, 3, and 4, respectively.

TABLE 4. ACCURACY ASSESSMENT RESULTS

		Accuracy Statistics		*t* Statistics	
Classification Methods	Data Used	*r*	*MAE*	*t*	Sig.
Regression Method	Only Ikonos Data	0.915	10.913		
	Ikonos and Temperature Data	0.918	10.622	1.408	0.161
ANN Method	Only Ikonos Data	0.924	12.208		
	Ikonos and Temperature Data	0.930	9.217	4.461	0.000
Regression Tree Method	Only Ikonos Data	0.939	8.307		

(r = 0.930, *MAE* = 9.217), suggesting that temperature played a significant role in better estimating impervious surface. For the regression tree method, Landsat-derived information was not significant enough to be included in the model. These results suggest that Landsat-derived information, in particular brightness temperature, does help in impervious surface estimation, especially with the ANN method.

Comparison between Linear Regression Analysis and Non-linear Models

In addition to examining the contribution from Landsat-derived information, the performances of the three models were also evaluated. Results (see Table 5 and Figure 8) indicate that regression tree has the best performance, with the highest Pearson's r value (0.939) and lowest *MAE* (8.307). ANN has a slightly poorer performance (r = 0.930, *MAE* = 9.217), and regression analysis has the worst accuracy, with the lowest Pearson's r (0.918) and highest *MAE* (10.622). Statistically, the paired sample t-test result (see Table 5) reveals that the accuracy of regression analysis is significantly lower than that of ANN (t = 2.600, p = 0.010) and regression tree method (t = 4.950, p = 0.000). When ANN and regression tree models were compared, however, no significant differences were found (t = 1.530, and p = 0.129). These results indicate that non-linear methods, including ANN and regression tree, perform significantly better than the linear method (regression modeling), while there are no significant differences between these two non-linear methods. However, as the differences are very small, the better accuracy achieved by the non-linear methods could be associated with model over-fitting.

Conclusions

This study attempts to integrate spectral information derived from Landsat-7 ETM+ imagery with Ikonos imagery to derive high-resolution impervious surface information. In particular, brightness temperature and NDWI derived from the Landsat-7 ETM+ image, and Tasseled Cap components and fractal dimension extracted from the Ikonos image were integrated for better estimation of impervious surface information. Three popular sub-pixel estimation methods, including linear regression modeling, artificial neural network and regression tree, were developed and compared using a paired t-test statistic.

A careful evaluation of both the linear and non-linear models suggests that the Tasseled Cap components of the Ikonos image are helpful in estimating sub-pixel imperviousness. Tasseled Cap component 2 (greenness) which is inversely related to impervious surface and Tasseled Cap component 3 (wetness) which is related to soil moisture are found to be statistically significant independent variables in the linear regression model. They were also found to be the major predictors of the regression tree and ANN models. Unlike the Landsat Tasseled Cap components, in which only the greenness (TC2) significantly contributes to the estimation of impervious surface, for Ikonos Tasseled Cap components, both greenness (TC2) and wetness (TC3) are important in explaining the variation of imperviousness. Apart from Tasseled Cap component 2 and 3 of the Ikonos image, the brightness temperature extracted for the Landsat-7 ETM+ image was found to be important to some extent in the regression and ANN model. In the regression tree method, brightness temperature was not significant for estimating imperviousness. For all the three methods, contrary to the expectation, the fractal dimension obtained from Ikonos image and NDWI obtained from Landsat-7 ETM+ were not significant in estimating sub-pixel imperviousness.

Moreover, comparative analysis of modeling results suggests that the regression tree approach yielded best results in comparison to the linear regression method and the non-linear ANN classification approach. Moreover, results indicate that non-linear methods, including ANN and regression tree, perform significantly better than the linear method (regression modeling), while there are no significant differences between these two non-linear methods. However, as the differences are very small, the better accuracy achieved by the non-linear methods could be associated with model over-fitting. Therefore, to make a generalization that non-linear methods are better than the linear regression analysis, there is a need to test the models in larger unsampled areas of the same image. This is not possible in this research as the study area is small and the larger Ikonos image was not available. Future studies could explore these techniques to estimate impervious surface by integrating Ikonos and Landsat ETM+ data specifically the TIR and SWIR bands in different geographical areas.

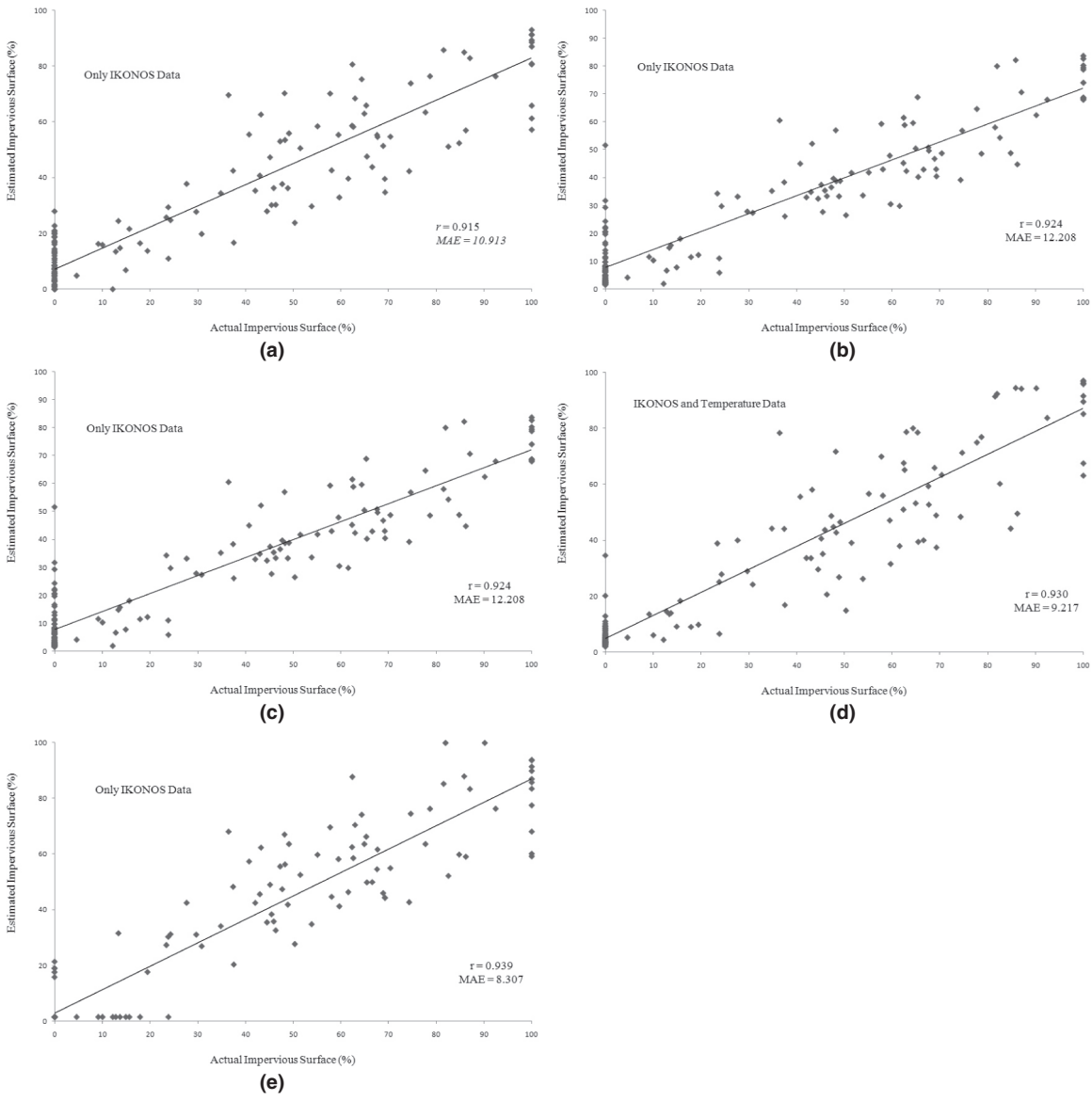

Figure 8. Regression plots of actual impervious surface percentage (%) versus estimated impervious surface percentage (%) of regression result (8a and 8b), neural network result (8c and 8d), and regression tree result (8e)

TABLE 5. MODEL COMPARISON (PAIRED SAMPLE *t*-test)

		Paired Sample Statistics		Paired Differences			
		Mean	Std. Deviation	Mean	Std. Deviation	*t*	Sig. (2-tailed)
Pair 1	RGR	10.622	9.138	1.40	6.63	2.60	0.010
	ANN	9.217	9.057				
Pair 2	RGR	10.622	9.138	2.31	5.73	4.95	0.000
	RT	8.307	9.098				
Pair 3	ANN	9.217	9.057	0.91	7.30	1.53	0.129
	RT	8.307	9.098				

Where RGR, ANN, and RT is the Regression, Artificial Neural Network, and Regression Tree method, respectively.

Acknowledgments

This research was supported by the United States' National Science Foundation Grant BCS-0822155 and the University of Wisconsin-Milwaukee Graduate School Research Committee Awards. Thanks to the anonymous reviewers for their suggestions on the earlier draft of this manuscript.

References

Aitkenhead, M.J., S. Flaherty, and M.E.J. Cutler, 2008. Evaluating neural networks and evidence pooling for land cover mapping, *Photogrammetric Engineering & Remote Sensing*, 74(8):1019–1032.

Arnold, C.L., and C.J. Gibbons, 1996. Impervious surface coverage - The emergence of a key environmental indicator, *Journal of the American Planning Association*, 62(2):243–258.

Bauer, M.E., N.J. Heinert, J.K. Doyle, and F. Yuan, 2004. Impervious surface mapping and change monitoring using satellite remote sensing, *Proceedings of the American Society for Photogrammetry and Remote Sensing 2004 Annual Conference*, 24–28 May, Denver, Colorado, unpaginated CD ROM.

Breiman, L., J.H. Friedman, R.A. Olshen, and C.J. Stone, 1984. *Classification and Regression Trees*, Wadsworth, Inc., Belmont, California (Since 1993 this book has been published by Chapman and Hall, New York).

Cablk, M.E., and T.B. Minor, 2003. Detecting and discriminating impervious cover with high resolution IKONOS data using principal component analysis and morphological operators, *International Journal of Remote Sensing*, 24(23):4627–4645.

Carlson, T., 2003. Preface - Applications of remote sensing to urban problems, *Remote Sensing of Environment*, 86(3):273–274.

Chabaeva, A., D.L. Civco, and J.D. Hurd, 2009. Assessment of impervious surface estimation techniques, *Journal of Hydrologic Engineering*, 14(4):377–387.

Civco, D.L., and J.D. Hurd, 1997. Impervious surface mapping for the state of Connecticut, *Proceedings of the ASPRS/ACCM 1997 Annual Convention*, Seattle, Washington, pp 124–135.

Civco, D.L., J.D. Hurd, E.H. Wilson, C.L. Arnold, and M.P. Prisloe, 2002. Quantifying and describing urbanizing landscapes in the Northeast United States, *Photogrammetric Engineering & Remote Sensing*, 68(10):1083–1090.

Dougherty, M., R.L. Dymond, S. Goetz, C.A. Jantz, and N. Goulet, 2004. Evaluation of impervious surface estimates in a rapidly urbanizing watershed, *Photogrammetric Engineering & Remote Sensing*, 70(11):1275–1284.

Eastman, J.R., 1985. Single-pass measurement of the fractional dimensionality of digitized cartographic lines, *Proceedings of the Canadian Cartographic Association Annual Meeting*, Fredericton, New Brunswick, Canada.

Eastman, J.R., 2003. *IDRISI Kilimanjaro, Guide to GIS and Image Processing*, Manual Version 14, Clark University Press, Massachusetts.

Elvidge, C.D., C. Milesi, J.B. Dietz, B.T. Tuttle, P.C. Sutton, R. Nemani, and J.E. Vogelmann, 2004. U.S. constructed area approaches the size of Ohio, *EOS Transactions*, 85(24):233–240.

Emerson, C.W., N.S.N. Lam, and D.A. Quattrochi, 1999. Multi-scale fractal analysis of image texture and pattern, *Photogrammetric Engineering & Remote Sensing*, 65(1):51–61.

Esch, T., V. Himmler, G. Schorcht, M. Thiel, T. Wehrmann, F. Bachofer, C. Conrad, M. Schmidt, and S. Dech, 2009. Large-area assessment of impervious surface based on integrated analysis of single-date Landsat-7 images and geospatial vector data, *Remote Sensing of Environment*, 113(8):1678–1690.

Flanagan, M., and D.L. Civco, 2001. Imagine subpixel classifier, Version 3.4. *Photogrammetric Engineering & Remote Sensing*, 67(1):23–28.

Gao, B.C., 1996. NDWI - A normalized difference water index for remote sensing of vegetation liquid water from space, *Remote Sensing of Environment*, 58(3):257–266.

Goetz, S.J., R.K. Wright, A.J. Smith, E. Zinecker, and E. Schaub, 2003. IKONOS imagery for resource management: Tree cover, impervious surfaces, and riparian buffer analyses in the mid-Atlantic region, *Remote Sensing of Environment,* 88(1):195–208.

Hasse, J.E., and R.G. Lathrop, 2003. Land resource impact indicators of urban sprawl, *Applied Geography*, 23(2/3):159–175.

Herold, M., D.A. Roberts, M.E. Gardner, and P.E. Dennison, 2004. Spectrometry for urban area remote sensing - Development and analysis of a spectral library from 350 to 2400 nm, *Remote Sensing of Environment,* 91(3/4):304–319.

Hester, D.B., H.I. Cakir, S.A.C. Nelson, and S. Khorram, 2008. Per-pixel classification of high spatial resolution satellite imagery for urban land-cover mapping, *Photogrammetric Engineering & Remote Sensing*, 74(4):463–471.

Horne, H.J., 2003. A Tasseled cap transformation for Ikonos images, *Proceedings of the American Society for Photogrammetry and Remote Sensing 2003 Annual Conference*, Anchorage, Alaska.

Jackson, T.J., D.Y. Chen, M. Cosh, F.Q. Li, M. Anderson, C. Walthall, P. Doriaswamy, and E.R. Hunt, 2004. Vegetation water content mapping using Landsat data derived normalized difference water index for corn and soybeans, *Remote Sensing of Environment*, 92(4):475–482.

Jensen, J.R., 2007. *Remote Sensing of the Environment: An Earth Resource Perspective*, Prentice Hall, Upper Saddle River, New Jersey, 592 p.

Ji, C.Y., 2000. Land-use classification of remotely sensed data using kohonen self-organizing feature map neural networks, *Photogrammetric Engineering & Remote Sensing*, 66(12):1451–1460.

Kauth, R.J., and G.S. Thomas, 1976. The tasseled cap - A graphic description of the spectral-temporal development of agricultural crops as seen in Landsat, *Proceedings of the Symposium on Machine Processing of Remotely Sensed Data*, 29 June – 01 July 1,West Lafayette, Indiana, pp 41–51.

Kavzoglu, T., and P.M. Mather, 2003. The use of backpropagating artificial neural networks in land cover classification, *International Journal of Remote Sensing*, 24(23):4907–4938.

Liu, W., and E.Y. Wu, 2005. Comparison of non-linear mixture models: Sub-pixel classification, *Remote Sensing of Environment*, 94(2):145–154.

Lu, D.S., and Q.H. Weng, 2006. Spectral mixture analysis of ASTER images for examining the relationship between urban thermal features and biophysical descriptors in Indianapolis, Indiana, USA, *Remote Sensing of Environment*, 104(2):157–167.

Lu, D.S., and Q.H. Weng, 2009. Extraction of urban impervious surfaces from an IKONOS image, *International Journal of Remote Sensing*, 30(5/6):1297–1311.

Mandelbrot, B.B., 1982. *The Fractal Geometry of Nature*, W. H. Freeman and Co., New York, 468 p.

Mertens, K.C., L.P.C. Verbeke, T. Westra, and R.R. De Wulf, 2004. Sub-pixel mapping and sub-pixel sharpening using neural network predicted wavelet coefficients, *Remote Sensing of Environment*, 91(2):225–236.

Mesev, V., 1997. Remote sensing of urban systems; Hierarchical integration with GIS, *Computer Environment and Urban Systems*, 21(3/4):175–187.

Mohapatra, R.P., and C.S. Wu, 2007. Sub-pixel imperviousness estimation with IKONOS image: An artificial neural network approach, *Remote Sensing of Impervious Surfaces* (Q. Weng, editor), CRC Press, Taylor & Francis Group, New York, pp. 21–38.

Powell, S.L., W.B. Cohen, Z. Yang, J.D. Pierce, and M. Alberti, 2008. Quantification of impervious surface in the Snohomish Water Resources Inventory Area of Western Washington from 1972–2006, *Remote Sensing of Environment*, 112(4):1895–1908.

Quinlan, J.R., 1993. Combining instance-based and model-based learning, *Proceedings of the 10th* International Conference of Machine Learning (P. Utgoff, edtor), Morgan Kaufmann Publishers, Amherst, Massachusetts, pp. 236–243.

Small, C., 2003. High spatial resolution spectral mixture analysis of urban reflectance, *Remote Sensing of Environment*, 88(1/2):170–186.

Southeastern Wisconsin Regional Planning Commission (SEWRPC), 2004. The population of Southeastern Wisconsin, Technical

Report #11, Fourth edition, URL: *http://www.sewrpc.org/publications/techrep/tr- 011_population_southeastern_wisconsin.pdf* (last date accessed: 18 August 2010).

Thomas, N., C. Hendrix, and R.G. Congalton, 2003. A comparison of urban mapping methods using high-resolution digital imagery, *Photogrammetric Engineering & Remote Sensing*, 69(9):963–972.

U.S. Census Bureau, 2000. Census 2000 Summary File 1 (SF 1) 100-Percent Data Geographic Comparison Tables URL:*http://factfinder.census.gov* (last date accessed: 18 August 2010).

U.S. Environmental Protection Agency (EPA), 2008. EPA's 2008 Report on the Environment, National Center for Environmental Assessment, Washington, D.C., EPA/600/R-07/045F, URL: *http://www.epa.gov/roe*, National Technical Information Service, Springfield, Virginia (last date accessed: 18 August 2010).

Wang, L., J.L. Silvan-Cardenas, and W.P. Sousa, 2008. Neural network classification of mangrove species from multi-seasonal Ikonos imagery, *Photogrammetric Engineering & Remote Sensing*, 74(7):921–927.

Warner, T.A., and F. Nerry, 2009. Does single broadband or multispectral thermal data add information for classification of visible, near- and shortwave infrared imagery of urban areas?, *International Journal of Remote Sensing*, 30(9):2155–2171.

Weng, Q.H., and D.S. Lu, 2008. A sub-pixel analysis of urbanization effect on land surface temperature and its interplay with impervious surface and vegetation coverage in Indianapolis, United States, *International Journal of Applied Earth Observation and Geoinformation*, 10(1):68–83.

Weng, Q.H., and D.S. Lu, 2009. Landscape as a continuum: An examination of the urban landscape structures and dynamics of Indianapolis City, 1991–2000 by using satellite images, *International Journal of Remote Sensing*, 30(10):2547–2577.

Wu, C.S., 2004. Normalized spectral mixture analysis for monitoring urban composition using ETM plus imagery, *Remote Sensing of Environment*, 93(4):480–492.

Wu, C.S., 2009. Quantifying high-resolution impervious surfaces using spectral mixture analysis, *International Journal of Remote Sensing*, 30(11):2915–2932.

Xian, G., and M. Crane, 2006. An analysis of urban thermal characteristics and associated land cover in Tampa Bay and Las Vegas using Landsat satellite data, *Remote Sensing of Environment*, 104(2):147–156.

Xian, G., 2008. Satellite remotely-sensed land surface parameters and their climatic effects for three metropolitan regions, *Advances in Space Research*, 41(11):1861–1869.

Xian, G., and M. Crane, 2005. Assessments of urban growth in the Tampa Bay watershed using remote sensing data, *Remote Sensing of Environment*, 97(2):203–215.

Xian, G., M. Crane, and C. McMahon, 2008. Quantifying multi-temporal urban development characteristics in Las Vegas from Landsat and ASTER data, *Photogrammetric Engineering & Remote Sensing,* 74(4):473–481.

Xian, G., M. Crane, and J. Su, 2007. An analysis of urban development and its environmental impact on the Tampa Bay watershed, *Journal of Environmental Management*, 85(4):965–976.

Yang, L., C, Huang, C.G. Homer, B.K. Wylie, and M.J. Coan, 2003. An approach for mapping large-area impervious surfaces: Synergistic use of Landsat-7 ETM+ and high spatial resolution imagery, *Canadian Journal of Remote Sensing*, 29(2):230–240.

Yang, X.J., 2006. Estimating landscape imperviousness index from satellite imagery, *IEEE Geoscience and Remote Sensing Letters*, 3(1):6–9.

Yuan, F., and M.E. Bauer, 2006. Mapping impervious surface using high-resolution imagery: A comparison of object-based and per pixel classification, *Proceedings of the 2006 ASPRS Annual Conference*, 01–05 May, Reno, Neveda.

Yuan, F., and M.E. Bauer, 2007. Comparison of impervious surface area and normalized difference vegetation index as indicators of surface urban heat island effects in Landsat imagery, *Remote Sensing of Environment*, 106(3):375–386.

Yuan, F., C.S. Wu, and M.E. Bauer, 2008. Comparison of spectral analysis techniques for impervious surface estimation using Landsat imagery, *Photogrammetric Engineering & Remote Sensing*, 74(8):1045–1055.

Zhang, X., T. Zhong, K. Wang, and Z. Cheng, 2009. Scaling of impervious surface area and vegetation as indicators to urban land surface temperature using satellite data, *International Journal of Remote Sensing*, 30(4):841–859.

Zheng, J., L. Yan, K. He, and Y. Sun, 2005. The fractal method study to distinguish road and water from the IKONOS image, *Proceedings of International Geoscience and Remote Sensing Symposium*, Seoul, Korea, Volume 6, pp. 3822–3825.

Zhou, Y.Y., and Y.Q. Wang, 2008. Extraction of impervious, surface areas from high spatial resolution imagery by multiple agent segmentation and classification, *Photogrammetric Engineering & Remote Sensing*, 74(7):857–868.

Zhou, Y., and Y.Q. Wang, 2007. An assessment of impervious surface areas in Rhode Island, *Northeastern Naturalist,* 14(4):643–650.

(Received 24 September 2009; accepted 17 March 2010; final version 20 May 2010)

2010 *PE&RS* OFFPRINT ORDER FORM

This is the ONLY opportunity available to order additional offset printing quality copies of your article. *PE&RS* does not go back on press after the issue's publication. Offprints are only shipped when ordered; they are not complimentary. However, all authors will receive one complimentary copy of the *PE&RS* issue containing their article. This form should be completed as soon as the initial proof is received, and should be returned with payment for offprints and page charges to the Production Manager as indicated below

ARTICLE DESCRIPTION:

ARTICLE TITLE:_____

_____

AUTHOR(S): _____

Please refer to the price chart and conditions on the back of this form in order to complete the table below.

Quantity	Description	Amount
	Offprints	
	Journal Covers (actual issue cover)	
	Extra Pages @ $125 per page (each page over 7 journal pages, reference "Instructions to Authors".)	
	Electronic copy of article in PDF format @ $2.00 per page Will be emailed. No shipping charges.	
	Shipping (applies to offprints and covers only (see price chart and conditions on back of this form.)	
	TOTAL	

SHIPPING ADDRESS:

Name (please print): _____

Organization Name (if applicable): _____

Street Address: _____

City:_____ State/Province: _____ Zip Code/Postal Code:_____

Country: _____ E-mail: _____

Business Phone:_____ Business Fax: _____

METHOD OF PAYMENT:

Payments must be made in US dollars, drawn on a US bank, or appropriate credit card. Make checks payable to ASPRS. Keep a copy for your records.

❒ Visa ❒ MasterCard ❒ Discover ❒ American Express

❒ Check (print *PE&RS* issue date & manuscript # on check)

Do you need a receipt? Receipts will be emailed.

Email address_____

_____
Name on Credit Card

_____
Account Number Expires (MO/YR)

_____
Signature Date

_____
Phone number for person above

SEND THIS FORM ALONG WITH METHOD OF PAYMENT TO:

Production Manager, ASPRS, 5410 Grosvenor Lane, Suite 210, Bethesda, MD 20814-2160

Phone: 301-493-0290 x107, Fax: 301-493-0208

updated 06/10

CONDITIONS:

Offprints are only shipped when ordered; they are not complimentary. However, all authors will receive one complimentary copy of the *PE&RS* issue containing their article. Offprint prices are based on the number of pages in an article. Orders are restricted to the quantities listed below. If offprints are not ordered prior to the issue's publication, reprints may be provided in multiples of 100 at the customer's expense. Shipping prices are based on weight and must be added to offprint and journal cover prices for an order to be processed. If overnight delivery is required, customers must provide an account code for the expense of the service (please indicate carrier and account number in the itemized table next to "Shipping").

PRICES:

Please enter the price that corresponds to the quantity of offprints and/or covers being ordered on the front of this form.

Offprints and Covers	25	50	75	100*
Offprints (1 to 4 page article)	9.00	15.00	21.00	27.00
Offprints (5 to 8 page article)	15.00	27.00	39.00	51.00
Offprints (9 to 12 page article)	21.00	39.00	57.00	75.00
Offprints (13 to 16 page article)	27.00	51.00	75.00	99.00
Journal Covers	15.00	25.00	35.00	45.00
Cover sponsor Applies to Outside Front Cover image suppliers only	475.00 for 1000 covers and TOC			

***Additional offprints can be ordered in the incriments listed above for the prices listed. When ordering additional offprints, add 25% to postage costs listed below.**

POSTAGE:

Please enter the price that corresponds to the quantity of offprints and/or covers being ordered on the front of this form.

Domestic (UPS Ground)	25	50	75	100	Canada (Air Parcel Post)	25	50	75	100
Offprints (1-4 page article)	7.59	7.98	9.08	8.69	Offprints (1-4 page article)	19.14	20.78	21.45	22.11
Offprints (5-8 page article)	7.98	9.08	9.57	10.53	Offprints (5-8 page article)	20.68	22.11	22.11	23.87
Offprints (9-12 page article)	8.25	9.57	9.79	10.23	Offprints (9-12 page article)	21.45	23.87	26.57	28.82
Offprints (13-16 page article)	8.69	9.79	10.23	11.44	Offprints (13-16 page article)	22.11	25.74	28.82	31.96
Journal Covers	7.59	7.98	8.25	8.64	Journal Covers	19.14	20.68	21.45	22.11
Cover sponsor Applies to Outside Front Cover image suppliers only	70.00				Cover sponsor Applies to Outside Front Cover image suppliers only	Contact ASPRS for shipping prices.			
Mexico (Air Parcel Post)	25	50	75	100	Overseas (Air Parcel Post)	25	50	75	100
Offprints (1-4 page article)	22.39	23.87	24.75	27.12	Offprints (1-4 page article)	28.05	30.31	41.69	36.03
Offprints (5-8 page article)	24.11	27.12	30.64	34.50	Offprints (5-8 page article)	30.36	36.03	45.26	47.41
Offprints (9-12 page article)	25.52	30.69	36.03	40.26	Offprints (9-12 page article)	33.17	41.69	49.55	55.99
Offprints (13-16 page article)	27.12	34.60	40.26	45.98	Offprints (13-16 page article)	36.03	47.41	55.99	64.51
Journal Covers	22.33	23.87	25.52	27.12	Journal Covers	28.05	30.31	41.69	36.03
Cover sponsor Applies to Outside Front Cover image suppliers only	Contact ASPRS for shipping prices.				Cover sponsor Applies to Outside Front Cover image suppliers only	Contact ASPRS for shipping prices.			

Assignment of Copyright to ASPRS

Current copyright law requires that authors of papers submitted for publication in *Photogrammetric Engineering & Remote Sensing* transfer copyright ownership to the American Society for Photogrammetry and Remote Sensing before the paper may be published. Upon receipt of this form with your Master Proof, please complete this form and forward it to the Production Coordinator (address below).

Manuscript Title: _____

_____

Author(s): _____

_____

Assignment of Copyright in the above-titled work is made on (date) _____ from the above listed author(s) to the American Society for Photogrammetry and Remote Sensing, publisher of *Photogrammetric Engineering & Remote Sensing*.

In consideration of the Publisher's acceptance of the above work for publication, the author or co-author(s) hereby transfer(s) to the American Society for Photogrammetry and Remote Sensing the full and exclusive copyright to the work for all purposes for the duration of the copyright. I (we) understand that such transfer of copyright does not preclude specific personal use, provided that prior to said use, permission is requested from and granted by the American Society for Photogrammetry and Remote Sensing.

I (we) acknowledge that this paper has not been previously published, nor is it currently being considered for publication by any other organization.

_____

Author/co-author signatures

_____

Co-authors may fill out and submit this form separately (photocopies are acceptable) if desired; but all co-authors must sign either this or a separate form.

Special Note to U.S. Government Employees

Material prepared by U.S. Government employees as part of their official duties need not have the assignment of copyright transferred since such material is automatically considered as part of the public domain.

If your paper falls within this category please check the appropriate statement and sign below.

_____ This paper has been prepared wholly as part of my (our) official duties as (a) U.S. Government Employee(s). I (we) acknowledge that this paper has not previously been published, nor is it currently being considered for publication, by any other organization.

_____ This paper has been prepared partly in the course of my (our) official duties as (a) U.S. Government Employee(s). For any part(s) not prepared in the course of my (our) official duties, copyright is hereby transferred to the American Society for Photogrammetry and Remote Sensing. I (we) acknowledge that this paper has not previously been published, nor is it currently being considered for publication, by any other organization.

_____

Author/co-author signatures

_____

Please return this form to:
Production Coordinator, ASPRS
5410 Grosvenor Lane, Suite 210
Bethesda, MD 20814-2160
301-493-0290, 301-493-0208 (fax), www.asprs.org

2010 *PE&RS* COLOR ORDER FORM

Accepted manuscripts will not be released for publication until all color charges have been paid. Color payment should be made when final manuscript is returned for publication to the Manuscript Coordinator. Payment and this form must be mailed/faxed to the ASPRS Production Manager at the address below.

ARTICLE DESCRIPTION:

ARTICLE TITLE:_____

_____

AUTHOR(S): _____

MANUSCRIPT # (if applicable): _____ # OF COLOR IMAGES/FIGURES: _____

COLOR PRICES AND CONDITIONS:

	1	2	+ **
Color Plates in Manuscripts (quantity _____) *	1,000.00	1,650.00	575.00
Outside Front Cover (discounts for reserving more than one cover at a time. 50% non-refundable deposit is required at time of reservation.)	3,700.00		

*** For purposes of this form, a color plate is considered to be a plate that is numbered, even if it contains several parts, e.g. (a), (b), and so on.**
****There is a $575.00 per plate charge for each color plate over two (2).**

Quantity	Description	Amount
	Color Plates (# of pages with color images/figures)	
	Cover Image (50% deposit required at time of reservation)	
	TOTAL	

METHOD OF PAYMENT:

Accepted manuscripts with color images will not be released for publication until this form is received along with payment. Payments must be made in US dollars, drawn on a US bank, or appropriate credit card. Make checks payable to ASPRS. Keep a copy for your records.

❒ Visa ❒ MasterCard ❒ Discover ❒ American Express

❒ Check (print *PE&RS* issue date & manuscript # on check)

_____
Name on Credit Card

_____
Account Number Expires (MO/YR)

_____
Signature Date

_____
Phone number for person above

Do you need a receipt? Receipts will be emailed.

Email address_____

Name/Contact Information of author submitting this form:

Name: _____

Affiliation: _____

Address: _____

_____

_____

Phone: _____

Fax: _____

Email: _____

SEND THIS FORM ALONG WITH METHOD OF PAYMENT TO:

Production Manager, ASPRS, 5410 Grosvenor Lane, Suite 210, Bethesda, MD 20814-2160
301-493-0290 x107, 301-493-0208 (fax)